JOURNAL OF INTEGRAL EQUATIONS
AND APPLICATIONS
Volume 29, Number 1, Spring 2017

COMPARISON BETWEEN NUMERICAL METHODS APPLIED TO THE DAMPED WAVE EQUATION

A. AIMI, M. DILIGENTI AND C. GUARDASONI

Communicated by Francisco-Javier Sayas

ABSTRACT. For the numerical solution of Dirichlet-Neumann problems related to 1D damped wave propagation, from a numerical point of view, we compare the so-called energetic approach, considered here separately for boundary and finite element methods with classical finite difference schemes, both explicit and implicit. The analysis reveals the superiority of energetic approximations with respect to unconditional stability and accuracy with respect to any choice of discretization parameters.

1. Introduction. The study of wave propagation modeled by partial differential equations (PDEs) of hyperbolic type is frequently encountered in a variety of physical and engineering problems. For instance, in the design of antennas, the interaction with electromagnetic waves must be known; for earthquake analysis, elastodynamic wave propagation is essential. Also, the analysis of damping phenomena that occur, for example, in fluid dynamics and in kinetic theory, is of particular interest: the dissipation is generated by the interaction of waves with the propagation medium and is also closely related to the dispersion, as in interactions between water streams and surfaces waves [**7, 8, 12, 13, 23**].

The use of advanced numerical techniques to solve PDEs, such as the finite element method (FEM), for instance in structural mechanics, and finite difference (FD) methods, primarily for fluid flow calculations, is now well established.

2010 AMS *Mathematics subject classification.* Primary 65M06, 65M30, 65M38.
Keywords and phrases. Damped wave equation, energetic boundary element method, energetic finite element method, finite differences schemes.
Received by the editors on November 30, 2015, and in revised form on October 7, 2016.
DOI:10.1216/JIE-2017-29-1-5 Copyright ©2017 Rocky Mountain Mathematics Consortium

On the other hand, both frequency-domain and time-domain boundary element methods (BEM) can be used for hyperbolic boundary value problems [**9, 10, 17, 18, 22**]. Space-time BEM has the advantage that it directly yields the unknown time-dependent quantities. In this last approach, the construction of boundary integral equations (BIEs), via the representation formula in terms of single and double layer potentials, uses the fundamental solution of the hyperbolic PDE and jump relations, see e.g., [**2, 14, 15, 19, 24**]. For the numerical solution of these problems, one needs consistent approximations and accurate simulations, even on large time intervals. Numerical results have shown that the standard BEM formulation can be unstable in some applications [**2**]; to overcome this drawback, a great deal of research has been devoted to the study of stability of the dynamic BEM formulation.

For the numerical solution of the damped wave equation in 1D unbounded layered media, we have recently considered [**4, 6**] the extension of the so-called *energetic* BEM-FEM coupling, introduced for the undamped wave equation [**1, 3, 5**]. This approximation technique is based on a weak formulation directly expressed in the space-time domain, thus avoiding the use of the Laplace transform and its inversion.

Weak problems, both on the boundary and in the domain, are strictly related to the energy of the second-order hyperbolic problem at hand, involving the use of test functions, which belong to the same functional spaces where the related weak solutions are searched and derived with respect to time. Even if the use of time differentiated test functions is not a novelty in the framework of FEM (see [**16**] and, e.g., [**21**]), it has been successfully applied for the first time in [**2**], in the context of BEM.

The energetic approach applied to 1D multilayered media has revealed robust with respect to the variation of both PDE and discretization parameters, and the approximate solutions have been proved to be stable and convergent in the appropriate functional spaces. The interested reader is referred to [**6**] for theoretical details based on energy arguments. Here, taking into account a bounded domain, the aim of the present contribution is to compare, from a numerical point of view, the above mentioned energetic approach as originally introduced for the coupling in [**4, 6**] and considered here separately for BEM and

FEM, with classical finite difference schemes, both explicit and implicit in time.

The paper is structured as follows. In Section 2, the model problem and its energetic boundary and domain weak formulations are presented. Section 3 is devoted to subsequent BEM and FEM discretizations. In Section 4, we recall classical difference schemes applied to the model problem. In Section 5, several numerical results are presented and discussed. Conclusions are summarized in the last section.

2. Model problem and energetic approach. Let $\Omega = (0, L) \subset \mathbb{R}$ be an open, bounded 1D domain, modeling a 3D rod with a dimension the length along the x-direction, much greater than the remaining ones, with boundary

$$\Gamma_N := \{x : x = 0\} \quad \text{and} \quad \Gamma_D := \{x : x = L\}.$$

Having denoted by $u(x,t)$ the problem unknown, which depends on space and time, and with

$$p(x,t) := \frac{\partial u}{\partial \mathbf{n}_x}(x,t),$$

which depends on a unitary outward normal vector $\mathbf{n}_x$ with respect to the transversal section of the rod, we want to solve the following wave propagation model problem: for all $x \in \Omega$, for all $t \in [0,T]$,

$$\left(\frac{\partial^2 u}{\partial x^2} - \frac{1}{c^2}\ddot{u} - \frac{2D}{c^2}\dot{u} - \frac{P}{c^2}u\right)(x,t) = f(x,t), \tag{2.1}$$

$$u(x,0) = \dot{u}(x,0) = 0, \tag{2.2}$$

$$p(0,t) = \overline{p}(t), \qquad u(L,t) = \overline{u}(t), \tag{2.3}$$

where overhead dots indicate derivatives with respect to time, c is the propagation velocity of a perturbation inside the rod, $D > 0$ and $P > 0$ represent viscous and material damping coefficients, respectively, $\overline{p}(t)$ and $\overline{u}(t)$ are given functions, and $f(x,t)$ is the assigned PDE right-hand side. The unknown $u(x,t)$ is understood in a weak sense, i.e., $u \in H^1([0,T]; H^1(\Omega))$ with enforced Dirichlet boundary condition, i.e., $u|_{\Gamma_D} = \overline{u}$.

In order to approximate $u(x,t)$ using a BEM technique, we have to obtain a boundary integral reformulation of problem (2.1)–(2.3). For this purpose, using classical arguments **[11]**, let us consider the space-time integral representation formula:

(2.4)
$$u(x,t) = \sum_{\xi=0,L} (G(x,\xi;\cdot) * p(\xi,\cdot))(t) - \sum_{\xi=0,L} \left(\frac{\partial G(x,\xi;\cdot)}{\partial \mathbf{n}_\xi} * u(\xi,\cdot) \right)(t) - \int_\Omega (G(x,\xi;\cdot) * f(\xi,\cdot))(t)\, \mathrm{d}\xi, \quad x \in \Omega,\ t \in [0,T],$$

where $*$ denotes the time convolution product and $G(x,\xi;t-\tau)$ is the forward fundamental solution of the damped wave equation (2.1) on the real line, which is given by

$$G(x,\xi;t-\tau) = \frac{c}{2} e^{-D(t-\tau)} \widetilde{I}_0\,[x,\xi;t,\tau]\, H[c(t-\tau) - |x-\xi|] \tag{2.5}$$

with $H[\cdot]$ the Heaviside distribution and

$$\widetilde{I}_0[x,\xi;t,\tau] = I_0\left(\frac{\sqrt{D^2 - P}}{c} \sqrt{c^2(t-\tau)^2 - (x-\xi)^2} \right) \tag{2.6}$$

with $I_0(\cdot)$ the modified Bessel function of order 0. Further, let us consider the normal derivative of the representation formula (2.4):

(2.7)
$$p(x,t) = \sum_{\xi=0,L} \left(\frac{\partial G(x,\xi;\cdot)}{\partial \mathbf{n}_x} * p(\xi,\cdot) \right)(t) - \sum_{\xi=0,L} \left(\frac{\partial^2 G(x,\xi;\cdot)}{\partial \mathbf{n}_x \partial \mathbf{n}_\xi} * u(\xi,\cdot) \right)(t) - \int_\Omega \left(\frac{\partial G(x,\xi;\cdot)}{\partial \mathbf{n}_x} * f(\xi,\cdot) \right)(t)\, \mathrm{d}\xi, \quad x \in \Omega,\ t \in [0,T].$$

Of course, derivatives in equations (2.4) and (2.7) must be understood in a distributional sense.

At this stage, we must take the limit as $x \to L^-$ in equation (2.4) and $x \to 0^+$ in equation (2.7), rewriting the kernels

$$\frac{\partial G}{\partial \mathbf{n}_x},\ \frac{\partial G}{\partial \mathbf{n}_\xi},\ \frac{\partial^2 G}{\partial \mathbf{n}_x \partial \mathbf{n}_\xi},$$

by means of the relations

$$\frac{\partial \widetilde{I}_0[x,\xi;t,\tau]}{\partial x} = -\frac{\partial \widetilde{I}_0[x,\xi;t,\tau]}{\partial \xi} = \frac{\partial \widetilde{I}_0[x,\xi;t,\tau]}{\partial \tau} \frac{x-\xi}{c^2(t-\tau)}, \tag{2.8}$$

$$\frac{\partial \widetilde{H}[x,\xi;t,\tau]}{\partial x} = -\frac{\partial \widetilde{H}[x,\xi;t,\tau]}{\partial \xi} = \frac{\partial \widetilde{H}[x,\xi;t,\tau]}{\partial \tau}\frac{x-\xi}{c|x-\xi|}, \tag{2.9}$$

where we have set $\widetilde{H}[x,\xi;t,\tau] := H[c(t-\tau)-|x-\xi|]$. After some analytic computations, see also **[4, 6]**, problem (2.1)–(2.3) can be rewritten as a system of two BIEs in the boundary unknowns $p(L,t)$ and $u(0,t)$:

$$\begin{cases} \mathcal{V}p(L,t) + \mathcal{K}_0 u(0,t) = f_u(t), \\ \mathcal{K}_L p(L,t) + \mathcal{W}u(0,t) = f_p(t), \end{cases} \qquad t \in [0,T], \tag{2.10}$$

where

$$\begin{aligned}
(\mathcal{V}p)(L,t) &= c\int_0^t e^{-D(t-\tau)}\widetilde{I}_0[L,L;t,\tau]p(L,\tau)\,\mathrm{d}\tau \\
(\mathcal{K}_0 u)(0,t) &= L\sqrt{D^2-P}\int_0^{t-L/c} e^{-D(t-\tau)}\frac{\widetilde{I}_1[L,0;t,\tau]}{s(L;t,\tau)}u(0,\tau)\,\mathrm{d}\tau \\
&\quad + u\left(0,t-\frac{L}{c}\right)e^{-DL/c} \\
(\mathcal{K}_L p)(L,t) &= -L\sqrt{D^2-P}\int_0^{t-L/c} e^{-D(t-\tau)}\frac{\widetilde{I}_1[0,L;t,\tau]}{s(L;t,\tau)}p(L,\tau)\,\mathrm{d}\tau \\
&\quad - e^{-D(L/c)}p\left(L,t-\frac{L}{c}\right) \\
(\mathcal{W}u)(0,t) &= -\frac{\sqrt{D^2-P}}{c}\int_0^t e^{-D(t-\tau)}\frac{\widetilde{I}_1[0,0;t,\tau]}{t-\tau}\,\mathrm{d}\tau \\
&\quad + \frac{1}{c}\big(Du(0,t)+\dot{u}(0,t)\big)
\end{aligned}$$

and

$$\begin{aligned}
f_u(t) &= u(L,t) - c\int_0^{t-L/c} e^{-D(t-\tau)}\widetilde{I}_0[L,0;t,\tau]p(0,\tau)\,\mathrm{d}\tau \\
&\quad + c\int_\Omega\int_0^{t-(|L-\xi|/c)} e^{-D(t-\tau)}\widetilde{I}_0[L,\xi;t,\tau]f(\xi,\tau)\,\mathrm{d}\tau\mathrm{d}\xi \\
f_p(t) &= p(0,t) - \sqrt{D^2-P}\int_0^{t-L/c} e^{-D(t-\tau)}\frac{\widetilde{I}_1[0,L;t,\tau]}{s(L;t,\tau)}u(L,\tau)\,\mathrm{d}\tau \\
&\quad + \frac{L^2}{c^2}(D^2-P)^{3/2}\int_0^{t-L/c}\frac{e^{-D(t-\tau)}}{s(L;t,\tau)}\left[\frac{I_1(\nu)}{\nu}\right]'_{\nu=(\sqrt{D^2-P}/c)s(L;t,\tau)}
\end{aligned}$$

$$
\begin{aligned}
&\times u(L,\tau)\,\mathrm{d}\tau \\
&+ e^{-D(L/c)}\left[L\frac{D^2-P}{2c^2}+\frac{D}{c}\right]u\left(L,t-\frac{L}{c}\right) \\
&+ \frac{1}{c}e^{-D(L/c)}\dot{u}\left(L,t-\frac{L}{c}\right) \\
&- \sqrt{D^2-P}\int_\Omega \xi\int_0^{t-\xi/c} e^{-D(t-\tau)}\frac{\widetilde{I}_1[0,\xi;t,\tau]}{s(\xi;t,\tau)}f(\xi,\tau)\,\mathrm{d}\tau\,\mathrm{d}\xi \\
&- c\int_\Omega \widetilde{I}_0\left[0,\xi;t,t-\frac{\xi}{c}\right]f\left(\xi,t-\frac{\xi}{c}\right)\mathrm{d}\xi,
\end{aligned}
$$

with

$$
\widetilde{I}_1(x,\xi;t,\tau)=I_1\left(\frac{\sqrt{D^2-P}}{c}\sqrt{c^2(t-\tau)^2-(x-\xi)^2}\right),
$$

$I_1(\cdot)$ the modified Bessel function of order 1, and

$$
s(\xi;t,\tau):=\sqrt{c^2(t-\tau)^2-\xi^2}.
$$

Following **[2, 5, 6]**, the energetic weak formulation of system (2.10) reads:

find $p(L,t)\in L^2([0,T])$ *and* $u(0,t)\in H^1([0,T])$ *such that*

$$
\begin{cases}
\left\langle(\dot{\mathcal{V}}p),q\right\rangle+\left\langle(\dot{\mathcal{K}_0}u),q\right\rangle=\left\langle\dot{f}_u,q\right\rangle \\
\left\langle\mathcal{K}_L p,\dot{v}\right\rangle+\left\langle\mathcal{W}u,\dot{v}\right\rangle=\left\langle f_p,\dot{v}\right\rangle,
\end{cases}
\tag{2.11}
$$

where $\langle\cdot,\cdot\rangle$ is the classical $L^2([0,T])$ inner product and $q(t)$, $v(t)$ are test functions belonging to the same functional space of $p(L,t)$ and $u(0,t)$, respectively. In particular, the first equation in (2.10) has been differentiated with respect to time and projected with the $L^2([0,T])$ scalar product by means of functions belonging to $L^2([0,T])$, while the second equation in (2.10) has been projected with the $L^2([0,T])$ scalar product by means of functions belonging to $H^1([0,T])$ derived with respect to time.

For the energetic weak formulation of the differential problem (2.1)–(2.3), let us multiply the PDE (2.1) for the time derivative of the test function

$$
w(x,t)\in H^1([0,T];H^1_{\Gamma_D}(\Omega)),
$$

where

$$H^1_{\Gamma_D}(\Omega) := \{w \in H^1(\Omega) : w|_{\Gamma_D} = 0\}$$

and integrate by parts in space, obtaining:

$$-\mathcal{A}(u,w) + \langle \dot{w}(L,\cdot),\, p(L,\cdot)\rangle = \mathcal{F}(w) - \langle \dot{w}(0,\cdot),\, \overline{p}\rangle, \tag{2.12}$$

where

$$\mathcal{A}(u,w) := \int_0^T \int_\Omega \left(\frac{\partial \dot{w}}{\partial x}\frac{\partial u}{\partial x} + \frac{1}{c^2}\dot{w}\ddot{u} + \frac{2D}{c^2}\dot{v}\dot{u} + \frac{P}{c^2}\dot{w}u \right)(x,t)\, dx\, dt, \tag{2.13}$$

$$\mathcal{F}(w) := \int_0^T \int_\Omega \dot{w}(x,t) f(x,t)\, dx\, dt. \tag{2.14}$$

Let us remark that the weak problems (2.11) and (2.12) have been deduced in strict relation to the energy of the solution, defined at time instant t, as:

$$\mathcal{E}_\Omega(u,t) := \frac{1}{2\,c^2}\int_\Omega \left[\left(c\frac{\partial u(x,t)}{\partial x} \right)^2 + \dot{u}^2(x,t) + P\,u^2(x,t) + 4D\int_0^t \dot{u}^2(x,s)\, ds \right] dx. \tag{2.15}$$

3. Discretization. For time discretization, we introduce a uniform decomposition of the time interval $[0,T]$ with time steps $\Delta t = T/N_{\Delta t}$, $N_{\Delta t} \in \mathbb{N}^+$, generated by the $N_{\Delta t}+1$ time instants:

$$t_k = k\Delta t, \quad k = 0, \ldots, N_{\Delta t}$$

and, for both BEM and FEM, we choose piecewise constant shape functions for the time approximation of p and piecewise linear shape functions for the time approximation of u, although higher degree shape functions can be used. In particular, for $k = 0, \ldots, N_{\Delta t} - 1$, time shape functions for the approximation of p and u will be defined, respectively, as:

$$\begin{aligned} \overline{\psi}_k(t) &= H[t - t_k] - H[t - t_{k+1}], \\ \widehat{\psi}_k(t) &= R(t - t_k) - R(t - t_{k+1}), \end{aligned} \tag{3.1}$$

where

$$R(t - t_k) = \frac{t - t_k}{\Delta t} H[t - t_k]$$

is the ramp function. Further, for the space discretization in energetic FEM, we consider the bounded domain Ω, decomposed by means of a uniform mesh constituted by $N_{\Delta x}$ straight elements having length Δx.

The functional background involved in the weak formulation (2.12) mandates the choice of shape functions belonging to $C^0(\Omega)$ for the spatial approximation of u in Ω. Hence, we will choose piecewise linear continuous basis functions $\widehat{\varphi}_j(x)$, $j = 0, \ldots, N_{\Delta x}$, related to the space mesh introduced above.

Hence, approximate solutions of the weak problems at hand will be expressed as:

$$
\begin{aligned}
u(0,t) \approx \widetilde{u}(0,t) &= \sum_{k=0}^{N_{\Delta t}-1} \alpha_k \widehat{\psi}_k(t), \\
p(L,t) \approx \widetilde{p}(L,t) &= \sum_{k=0}^{N_{\Delta t}-1} \beta_k \overline{\psi}_k(t),
\end{aligned}
\tag{3.2}
$$

concerning the energetic BEM and

$$
u(x,t) \approx \widetilde{u}(x,t) = \sum_{k=0}^{N_{\Delta t}-1} \widehat{\psi}_k(t) \sum_{j=0}^{N_{\Delta x}-1} \gamma_{kj}\, \widehat{\varphi}_j(x) + \overline{u}(t) \widehat{\varphi}_{N_{\Delta x}}(x),
\tag{3.3}
$$

concerning the energetic FEM.

Let us note that both these discretizations produce their related final linear system:

$$
\mathrm{M}\,\mathrm{x} = \mathrm{y},
\tag{3.4}
$$

where matrix M has a block lower triangular Toeplitz structure with blocks dependent on the difference $t_h - t_k$, so that they vanish if $t_h < t_k$, as frequently pointed out in previous papers, see **[1, 3, 5]**. Finally, we remark that, in energetic BEM, at every time step the only discrete unknowns reduce to α_k and β_k coefficients since we need only approximate $u(0,t)$ and $p(L,t)$.

Concerning stability and convergence of both BEM and FEM energetic approaches, these properties can be derived from theoretical results obtained in **[6]** for their coupling. In that paper, a slightly dissipative character of the energetic discretization was pointed out. In

particular, having set

$$\|\cdot\| = \|\cdot\|_{L^2(\Omega)}, \qquad \widetilde{u}(\cdot, t_h) = u^h,$$

and having introduced the discrete energy in Ω at the time instant t_h as

(3.5)
$$\mathcal{E}_\Omega^h := \frac{1}{2c^2}\left[c^2\|(u^h)'\|^2 + \left\|\frac{u^h - u^{h-1}}{\Delta t}\right\|^2 + P\|u^h\|^2 + 4D\Delta t\sum_{k=0}^{h}\left\|\frac{u^k - u^{k-1}}{\Delta t}\right\|^2\right],$$

it turns out that $\mathcal{E}_\Omega^{h+1} = \mathcal{E}_\Omega^h + \mathcal{O}((\Delta t)^2)$, and this is also valid for the pure wave equation without damping terms, simply forcing $P = D = 0$ in the definition of both continuous (2.15) and discrete (3.5) energy.

4. Classical difference schemes. In numerical examples below, we will compare the energetic approach with the following finite difference schemes:

• a second order centered finite differences (CFD) scheme in time and in space, approximating $u_j^k := u(x_j, t_k)$ by $\widetilde{u}_j^k$. Assuming adequate regularity of the solution $u(x,t)$, from equation (2.1), we derive

(4.1)
$$\frac{u_{j+1}^k - 2u_j^k + u_{j-1}^k}{\Delta x^2} - \frac{u_j^{k+1} - 2u_j^k + u_j^{k-1}}{c^2\Delta t^2} - \frac{D}{c^2}\frac{u_j^{k+1} - u_j^{k-1}}{\Delta t} - \frac{P}{c^2}u_j^k + \mathcal{O}(\Delta x^2) + \mathcal{O}(\Delta t^2) = f(x_j, t_k).$$

Defining $\lambda := c(\Delta t/\Delta x)$, the next algorithm has been developed to evaluate $\widetilde{u}_j^k$, for $j = 0, \ldots, N_{\Delta x} - 1$ and $k = 1, \ldots, N_{\Delta t}$:

– at the first time step $t_1 = \Delta t$,

$$\widetilde{u}_j^1 = -c^2\Delta t^2 f(x_j, 0), \quad \text{for } j = 1, \ldots, N_{\Delta x} - 1,$$

obtained by relations

$$\widetilde{u}_j^1 = u_j^0 + \Delta t\,\dot{u}_j^0 + \frac{\Delta t^2}{2}\,\ddot{\widetilde{u}}_j^0$$
$$\ddot{\widetilde{u}}_j^0 = c^2\frac{u_{j+1}^0 - 2u_j^0 + u_{j-1}^0}{\Delta x^2} - 2D\dot{u}_j^0 - Pu_j^0 - c^2 f(x_j, 0)$$

and exploiting the initial conditions which imply $u_j^0 = \dot{u}_j^0 = 0$;

– then, for $k = 1, \dots, N_{\Delta t} - 1$,

$$\widetilde{u}^{k+1}_{N_{\Delta x}} = \overline{u}(t_{k+1})$$

$$\widetilde{u}^{k+1}_j = \frac{1}{1 + D\Delta t}\Big\{\lambda^2\widetilde{u}^k_{j+1} + \lambda^2\widetilde{u}^k_{j-1} + (2 - 2\lambda^2 - P\Delta t^2)\widetilde{u}^k_j + (D\Delta t - 1)\widetilde{u}^{k-1}_j - c^2\Delta t^2 f(x_j, t_k)\Big\},$$

$$\text{for } j = 1, \dots, N_{\Delta x} - 1,$$

$$\widetilde{u}^{k+1}_0 = \frac{1}{1+D\Delta t}\Big\{\lambda^2\widetilde{u}^k_1 + (2 - 2\lambda^2 - P\Delta t^2)\tilde{u}^k_0 + \lambda^2(\widetilde{u}^k_1 + 2\Delta x\overline{p}(t_k)) + (D\Delta t - 1)\widetilde{u}^{k-1}_0 - c^2\Delta t^2 f(0, t_k)\Big\}$$

where, for $j = 0$, we introduce the *ghost point* $x_{-1} := x_0 - \Delta x$ and the second order approximation using the Neumann boundary condition:

$$\widetilde{u}^k_{-1} = \widetilde{u}^k_1 + 2\,\Delta x\,\overline{p}(t_k).$$

This scheme is stable under the well-known CFL condition $\lambda \leq 1$.

• an implicit finite differences (IFD) second order scheme obtained by replacing u^k_j with the mean value $(u^{k+1}_j + u^{k-1}_j)/2$ in the terms of equation (4.1) where no time derivatives are involved.

The first time step is developed as in CFD; then this method results in solving the following linear systems, for $k = 1, \dots, N_{\Delta t} - 1$:

$$Mu^{k+1} = -c^2\Delta t^2 F^k + 2u^k + \widetilde{M}u^{k-1} + \widetilde{F}^k,$$

where

$$M = \begin{pmatrix} \alpha & -\lambda^2 & 0 & \cdots & 0 \\ -\lambda^2/2 & \alpha & -\lambda^2/2 & \cdots & 0 \\ 0 & -\lambda^2/2 & \alpha & \cdots & 0 \\ \vdots & \vdots & \ddots & \ddots & \vdots \\ 0 & 0 & \cdots & -\lambda^2/2 & \alpha \end{pmatrix},$$

with $\alpha = 1 + D\Delta t + P\Delta t^2/2 + \lambda^2$, is a strictly diagonally dominant

matrix and therefore invertible, $\widetilde{\mathrm{M}} = -\mathrm{M} + 2D\,\Delta t\,\mathrm{I}$ and

$$u^k = \begin{pmatrix} \widetilde{u}_0^k \\ \widetilde{u}_1^k \\ \vdots \\ \widetilde{u}_{N_{\Delta x}-2}^k \\ \widetilde{u}_{N_{\Delta x}-1}^k \end{pmatrix},$$

$$\mathrm{F}^k = \begin{pmatrix} f(0,t_k) \\ f(x_1,t_k) \\ \vdots \\ f(x_{N_{\Delta x}-2},t_k) \\ f(x_{N_{\Delta x}-1},t_k) \end{pmatrix},$$

$$\widetilde{\mathrm{F}}^k = \frac{\lambda^2}{2} \begin{pmatrix} 2\Delta x(\overline{p}(t_{k+1}) + \overline{p}(t_{k-1})) \\ 0 \\ \vdots \\ 0 \\ \overline{u}(t_{k+1}) + \overline{u}(t_{k-1}) \end{pmatrix}.$$

This method is expected to be unconditionally stable.

5. Numerical results. In the first two examples we compare the above numerical methods by applying them to some benchmarks chosen in such a way that the related reference solutions reproduce the same challenging features which cause trouble in elliptic 1D advection-diffusion-reaction problems, see **[20]**. The last example is dedicated to the analysis of long-time behavior of the energetic approaches, showing their stability and convergence.

Example 5.1. Let us set $L = 1$, $T = 1$ and propagation velocity $c = 1$. At first, let us consider the case $P = 0$ and the differential problem (2.1)–(2.3) with exact solution

$$u(x,t) = \frac{e^{-2Dc^2t^2} - 1}{e^{-2D} - 1}(1-x)^3, \quad 0 \le x \le 1;\ t \in [0,1]. \tag{5.1}$$

For all $x \in [0,1]$, the following occurs:

• if $D \ll 1$, then $u(x,t) \approx c^2t^2(1-x)^3$ as, for example, is observable in Figure 2;

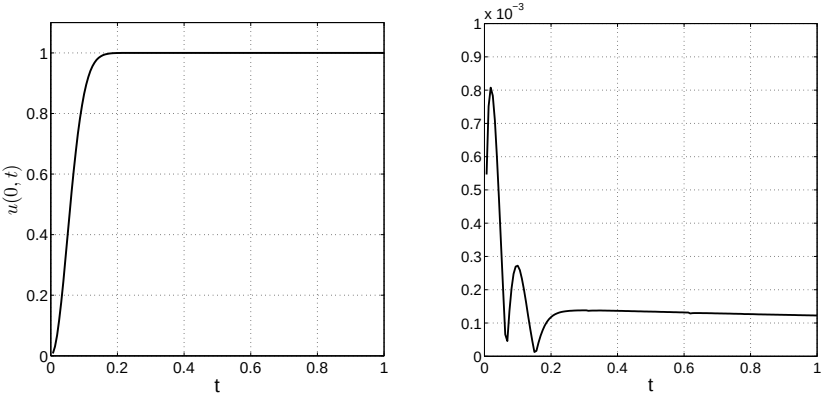

FIGURE 1. Analytical solution and relative error obtained by energetic BEM with $c = 1$, $P = 0$, $D = 100$ and $\Delta t = 0.00625$.

• if $D \gg 1$, it is verified that $u(x,t) \approx (1-x)^3$ over the time interval $(0,1]$ but it must collate to 0 at $t = 0$ as, for example, is observable in Figure 4. In order to avoid oscillations in time due to the high gradient, it may occur that one must choose the discretization parameter $\Delta t < D^{-1}$, as it is usual in standard FEM for the numerical solution of 1D advection-diffusion equation in order to keep the Péclet number $\mathrm{Pe}_D := \Delta t D < 1$.

Taking energetic BEM into consideration, from Table 1 we observe that the numerical solution at $x = 0$ converges to the analytical solution $u(0,t)$. The relative errors written in Table 1 are defined as

$$E_s := \frac{\|\widetilde{u}(0,\cdot) - u(0,\cdot)\|_{L^2([0,1])}}{\|u(0,\cdot)\|_{L^2([0,1])}}, \tag{5.2}$$

where the numerical solutions $\widetilde{u}(0,\cdot)$ are computed by discretization parameters $\Delta t = 0.1 \times 2^{-s}$, $s = 0, \ldots, 4$. Errors increase with an increasing magnitude of D because of the introduction of a region with a higher and higher gradient, see Figure 1, but the rate of convergence is substantially equal to 2 independently from the choice of value D. In any case, even when $\Delta t > D^{-1}$ no instabilities appear.

Now considering $\widetilde{u}(0,\cdot)$ obtained by energetic FEM, see Table 2, the accuracy, as is well known, is lower and the rate of convergence tends to order 1 as estimated in **[6]**. Analyzing the behavior of the solution

TABLE 1. L_2 relative errors E_s of BEM solution with respect to the analytical solution (5.1) at $x = 0$ and $\mathcal{E}_s = \log_2(E_{s-1}/E_s)$.

BEM

$\Delta t = 0.1 \times 2^{-s}$

	$D = 10^{-1}$		$D = 1$		$D = 10$		$D = 100$	
s	E_s	$\mathcal{E}_s$	E_s	$\mathcal{E}_s$	E_s	$\mathcal{E}_s$	E_s	$\mathcal{E}_s$
0	$1.9{\cdot}10^{-4}$		$9.4{\cdot}10^{-4}$		$7.1{\cdot}10^{-3}$		$1.5{\cdot}10^{-2}$	
1	$4.8{\cdot}10^{-5}$	2.0	$2.3{\cdot}10^{-4}$	2.0	$1.6{\cdot}10^{-3}$	2.1	$1.5{\cdot}10^{-2}$	0.01
2	$1.2{\cdot}10^{-5}$	2.0	$5.9{\cdot}10^{-5}$	2.0	$4.0{\cdot}10^{-4}$	2.0	$3.1{\cdot}10^{-3}$	2.2
3	$3.0{\cdot}10^{-6}$	2.0	$1.5{\cdot}10^{-5}$	2.0	$1.0{\cdot}10^{-4}$	2.0	$7.2{\cdot}10^{-4}$	2.1
4	$7.6{\cdot}10^{-7}$	2.0	$3.7{\cdot}10^{-6}$	2.0	$2.5{\cdot}10^{-5}$	2.0	$1.8{\cdot}10^{-4}$	2.0

TABLE 2. L_2 relative errors E_s of FEM solution with respect to the analytical solution (5.1) at $x = 0$ and $\mathcal{E}_s = \log_2(E_{s-1}/E_s)$.

FEM

$\Delta t = \Delta x = 0.1 \times 2^{-s}$

	$D = 10^{-1}$		$D = 1$		$D = 10$		$D = 100$	
s	E_s	$\mathcal{E}_s$	E_s	$\mathcal{E}_s$	E_s	$\mathcal{E}_s$	E_s	$\mathcal{E}_s$
0	$3.4{\cdot}10^{-2}$		$2.6{\cdot}10^{-2}$		$2.1{\cdot}10^{-2}$		$8.4{\cdot}10^{-3}$	
1	$1.9{\cdot}10^{-2}$	0.85	$1.4{\cdot}10^{-2}$	0.90	$1.2{\cdot}10^{-2}$	0.86	$6.3{\cdot}10^{-3}$	0.42
2	$9.8{\cdot}10^{-3}$	0.93	$7.2{\cdot}10^{-3}$	0.95	$6.3{\cdot}10^{-3}$	0.90	$3.8{\cdot}10^{-3}$	0.74
3	$5.0{\cdot}10^{-3}$	0.97	$3.7{\cdot}10^{-3}$	0.97	$3.3{\cdot}10^{-3}$	0.94	$2.0{\cdot}10^{-3}$	0.90
4	$2.5{\cdot}10^{-3}$	0.98	$1.8{\cdot}10^{-3}$	0.99	$1.7{\cdot}10^{-3}$	0.97	$1.1{\cdot}10^{-3}$	0.94

over the whole domain $\Omega \times [0,1]$ (Figures 3, 5), we still note that the maximum relative error, defined as

$$\text{Err} := \frac{\max_{\Omega\times[0,1]} |\widetilde{u}(x,t) - u(x,t)|}{\max_{\Omega\times[0,1]} |u(x,t)|},$$

is higher in regions with a higher gradient. However, with energetic formulation, FEM keeps its stability even for $\Delta t > D^{-1}$ and without respect to any CFL condition (Figure 5) even when (refer to Table 3) D is large and we need to refine the time grid more than the space grid in order to improve accuracy due to the jump in gradient near $t = 0$.

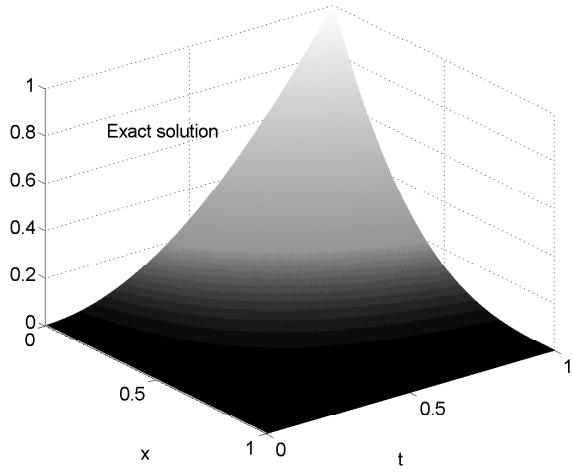

FIGURE 2. Exact solution (5.1) with $c = 1$ and $D = 0.1$.

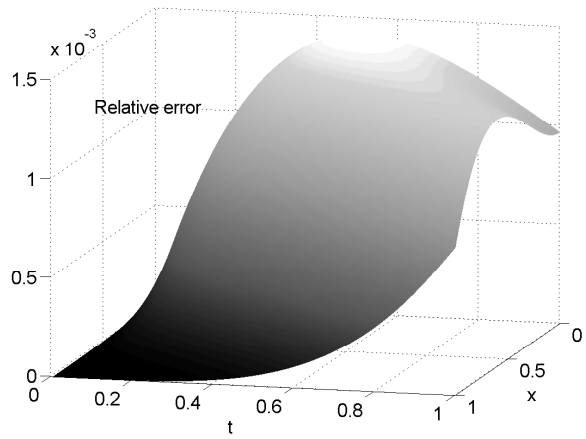

FIGURE 3. Relative error with respect to the solution in Figure 2 obtained by energetic FEM with $\Delta t = \Delta x = 0.00625$.

Considering either CFD or IFD, we obtain that the accuracy is of order 2 (see Tables 4 and 6, respectively, where a discrete L^2 norm has

TABLE 3. Maximum relative errors of FEM solution with respect to the analytical solution (5.1) over the entire grid, for $D = 100$.

Δt \ Δx	0.1	0.05	0.025	0.0125	0.00625
0.1	$2.05{\cdot}10^{-2}$	$1.79{\cdot}10^{-2}$	$1.75{\cdot}10^{-2}$	$1.75{\cdot}10^{-2}$	$1.74{\cdot}10^{-2}$
0.05	$2.12{\cdot}10^{-2}$	$1.81{\cdot}10^{-2}$	$1.79{\cdot}10^{-2}$	$1.77{\cdot}10^{-2}$	$1.77{\cdot}10^{-2}$
0.025	$1.63{\cdot}10^{-2}$	$1.65{\cdot}10^{-2}$	$1.63{\cdot}10^{-2}$	$1.64{\cdot}10^{-2}$	$1.64{\cdot}10^{-2}$
0.0125	$9.48{\cdot}10^{-3}$	$8.81{\cdot}10^{-3}$	$8.80{\cdot}10^{-3}$	$8.76{\cdot}10^{-3}$	$8.79{\cdot}10^{-3}$
0.00625	$6.88{\cdot}10^{-3}$	$4.89{\cdot}10^{-3}$	$4.91{\cdot}10^{-3}$	$4.89{\cdot}10^{-3}$	$4.88{\cdot}10^{-3}$

TABLE 4. L_2 relative errors E_s of CFD solution with respect to the analytical solution (5.1) at $x = 0$ and $\mathcal{E}_s := \log_2(E_{s-1}/E_s)$.

CFD

$\Delta t = \Delta x = 0.1 \times 2^{-s}$

	$D = 10^{-1}$		$D = 1$		$D = 10$		$D = 100$	
s	E_s	$\mathcal{E}_s$	E_s	$\mathcal{E}_s$	E_s	$\mathcal{E}_s$	E_s	$\mathcal{E}_s$
0	$2.4{\cdot}10^{-3}$		$2.8{\cdot}10^{-3}$		$5.2{\cdot}10^{-2}$		$5.1{\cdot}10^{-1}$	
1	$6.0{\cdot}10^{-4}$	2.0	$6.8{\cdot}10^{-4}$	2.1	$1.3{\cdot}10^{-2}$	2.0	$1.5{\cdot}10^{-1}$	1.7
2	$1.5{\cdot}10^{-4}$	2.0	$1.7{\cdot}10^{-4}$	2.0	$3.2{\cdot}10^{-3}$	2.0	$3.8{\cdot}10^{-2}$	2.0
3	$3.7{\cdot}10^{-5}$	2.0	$4.2{\cdot}10^{-5}$	2.0	$8.0{\cdot}10^{-4}$	2.0	$9.5{\cdot}10^{-3}$	2.0
4	$9.3{\cdot}10^{-6}$	2.0	$1.1{\cdot}10^{-5}$	2.0	$2.0{\cdot}10^{-4}$	2.0	$2.4{\cdot}10^{-3}$	2.0

TABLE 5. Maximum relative errors of CFD solution with respect to the analytical solution (5.1) over the whole grid, for $D = 100$.

Δt \ Δx	0.1	0.05	0.025	0.0125	0.00625
0.1	$9.11{\cdot}10^{-1}$				
0.05	$3.05{\cdot}10^{-1}$	$3.08{\cdot}10^{-1}$			
0.025	$5.83{\cdot}10^{-2}$	$5.80{\cdot}10^{-2}$	$5.75{\cdot}10^{-2}$		
0.0125	$1.49{\cdot}10^{-2}$	$1.47{\cdot}10^{-2}$	$1.46{\cdot}10^{-2}$	$1.44{\cdot}10^{-2}$	
0.00625	$3.70{\cdot}10^{-3}$	$3.66{\cdot}10^{-3}$	$3.62{\cdot}10^{-3}$	$3.59{\cdot}10^{-3}$	$3.58{\cdot}10^{-3}$

been considered). As expected, the solution obtained with CFD is affected by huge instabilities when the CFL condition is not verified, and therefore, the upper triangular part of Table 5 is empty. On the contrary, these instabilities do not appear with the IFD method; how-

ever, looking at the upper triangular part of Table 7, we observe that no significative improvements are achieved refining in space.

Analyzing the behavior of the numerical solution over the entire domain $\Omega \times [0,1]$ (Figures 7 and 8), we still note that the maximum relative error is higher in regions with higher gradient, and moreover, a significant contribution is due to the approximation of the normal derivative at $x = 0$. If $\mathrm{Pe}_D > 1$, it seems that (refer to Figure 9) at $t = 0$ some instabilities appear, but the dissipative nature of the problem smooths instead of amplifying them as happens in classical advection-diffusion boundary value problems.

Example 5.2. Let us again fix $L = 1$, $T = 1$, $c = 1$. Consider here the case $D = 0$ and the differential problem (2.1)–(2.3) with exact solution

$$u(x,t) = \frac{\sin(\sqrt{P}c^2t^2)}{\sin(\sqrt{P})}(1-x)^3, \quad 0 \le x \le 1\,; \quad t \in [0,1]. \tag{5.3}$$

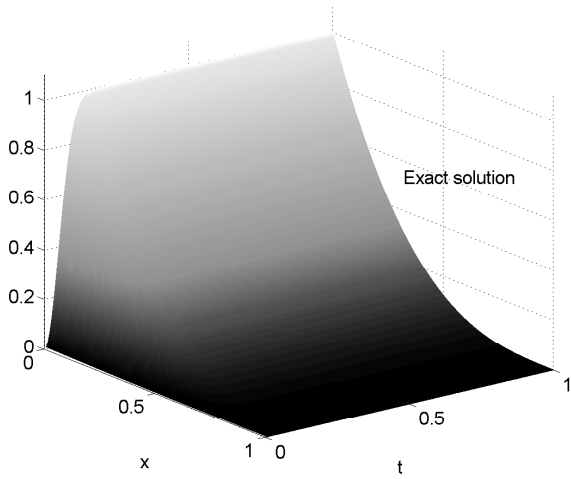

FIGURE 4. Exact solution (5.1) with $c = 1$ and $D = 100$.

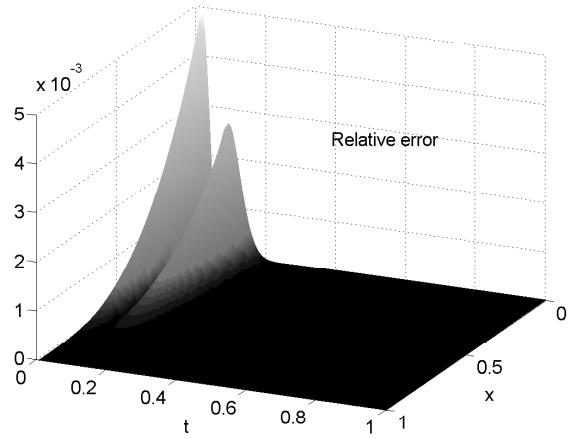

FIGURE 5. Relative error with respect to the solution in Figure 4 obtained by energetic FEM with $\Delta t = \Delta x = 0.00625$.

TABLE 6. L_2 relative errors E_s of IFD solution with respect to the analytical solution (5.1) at $x = 0$ and $\mathcal{E}_s := \log_2(E_{s-1}/E_s)$.

IFD

$\Delta t = \Delta x = 0.1 \times 2^{-s}$

	$D = 10^{-1}$		$D = 1$		$D = 10$		$D = 100$	
s	E_s	$\mathcal{E}_s$	E_s	$\mathcal{E}_s$	E_s	$\mathcal{E}_s$	E_s	$\mathcal{E}_s$
0	$1.6{\cdot}10^{-2}$		$1.2{\cdot}10^{-2}$		$5.3{\cdot}10^{-2}$		$5.1{\cdot}10^{-1}$	
1	$4.2{\cdot}10^{-3}$	1.9	$3.3{\cdot}10^{-3}$	1.9	$1.3{\cdot}10^{-2}$	2.0	$1.5{\cdot}10^{-1}$	1.8
2	$1.1{\cdot}10^{-3}$	1.9	$8.7{\cdot}10^{-4}$	1.9	$3.3{\cdot}10^{-3}$	2.0	$3.8{\cdot}10^{-2}$	2.0
3	$2.8{\cdot}10^{-4}$	2.0	$2.2{\cdot}10^{-4}$	2.0	$8.2{\cdot}10^{-4}$	2.0	$9.5{\cdot}10^{-3}$	2.0
4	$7.0{\cdot}10^{-5}$	2.0	$5.6{\cdot}10^{-5}$	2.0	$2.1{\cdot}10^{-4}$	2.0	$2.4{\cdot}10^{-3}$	2.0

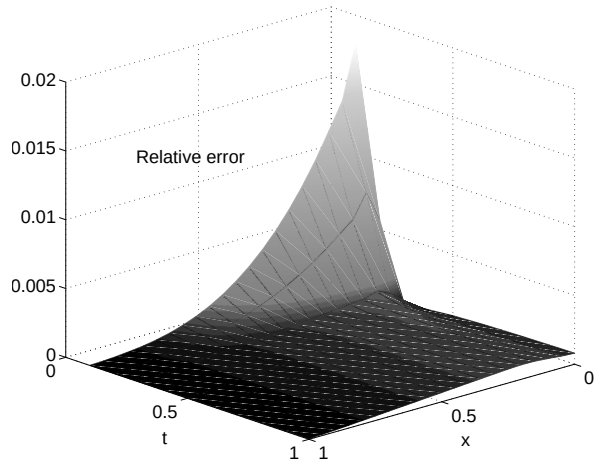

FIGURE 6. Relative error with respect to the solution in Figure 4 obtained by energetic FEM with $\Delta t = 0.1$, $\Delta x = 0.05$.

TABLE 7. Maximum relative errors of IFD solution with respect to the analytical solution (5.1) over the whole grid, for $D = 100$.

Δt \ Δx	0.1	0.05	0.025	0.0125	0.00625
0.1	$9.11{\cdot}10^{-1}$	1.02	1.08	1.11	1.12
0.05	$3.03{\cdot}10^{-1}$	$3.04{\cdot}10^{-1}$	$3.02{\cdot}10^{-1}$	$3.01{\cdot}10^{-1}$	$3.00{\cdot}10^{-1}$
0.025	$5.83{\cdot}10^{-2}$	$5.81{\cdot}10^{-2}$	$5.79{\cdot}10^{-2}$	$5.76{\cdot}10^{-2}$	$5.74{\cdot}10^{-2}$
0.0125	$1.49{\cdot}10^{-2}$	$1.48{\cdot}10^{-2}$	$1.46{\cdot}10^{-2}$	$1.45{\cdot}10^{-2}$	$1.44{\cdot}10^{-2}$
0.00625	$3.70{\cdot}10^{-3}$	$3.67{\cdot}10^{-3}$	$3.62{\cdot}10^{-3}$	$3.59{\cdot}10^{-3}$	$3.59{\cdot}10^{-3}$

Also, in this example, it happens that, for all $x \in [0, 1]$:

• if $P \ll 1$, then $u(x, t) \approx c^2 t^2 (1 - x)^3$ as, for example, is observable in Figure 12;

• if $P \gg 1$, $u(x, t)$ has a $(1 - x)^3$-like decay behavior over the time interval $(0, 1]$, but it must collate to 0 at $t = 0$. It is very oscillating in time when $x = 0$ as, for example, is observable in Figure 14. This case

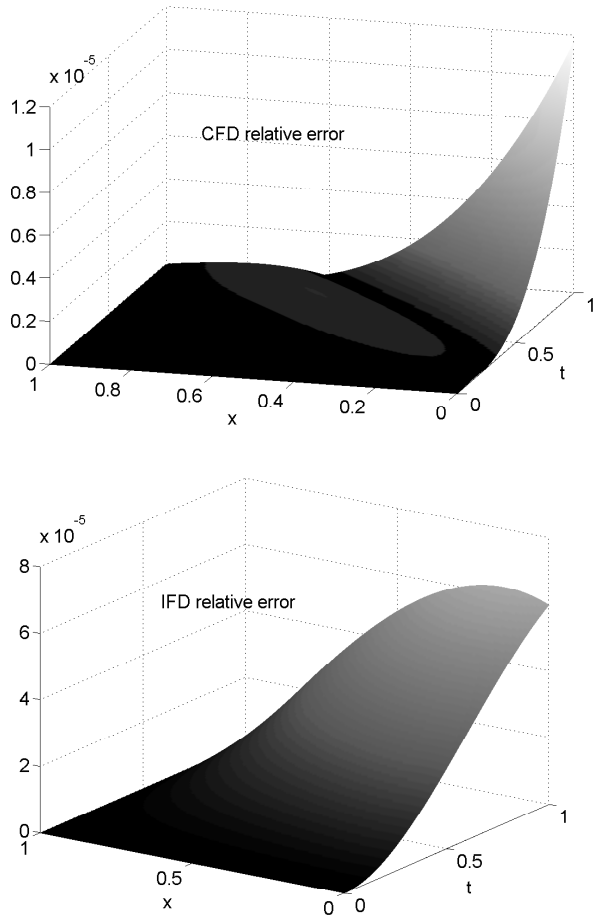

FIGURE 7. Relative error with respect to the exact solution (represented in Figure 2) obtained by CFD (above) and by IFD (below) with $\Delta t = \Delta x = 0.00625$.

has different difficulties with respect to the 1D reaction-diffusion equation but still dependent on the magnitude P.

Taking energetic BEM into consideration, from Table 8 we observe that the numerical solution at $x = 0$ converges to the analytical solution

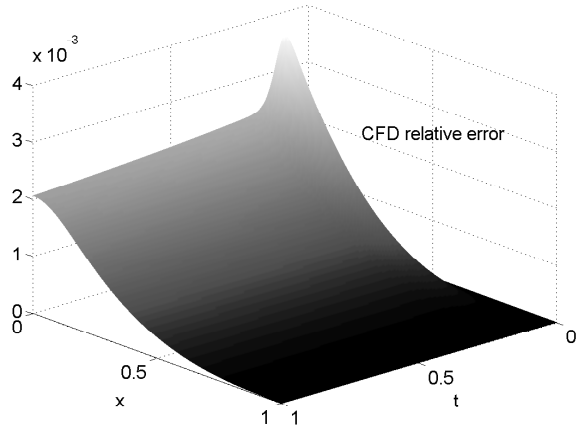

FIGURE 8. Relative error with respect to the exact solution (represented in Figure 4) obtained by CFD (the relative error obtained by IFD is analogous) with $\Delta t = \Delta x = 0.00625$.

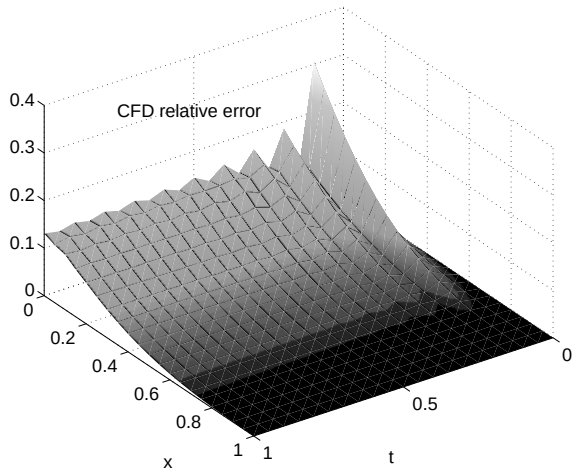

FIGURE 9. Relative error with respect to the exact solution (represented in Figure 4) obtained by CFD (the relative error obtained by IFD is analogous) with $\Delta t = \Delta x = 0.1$.

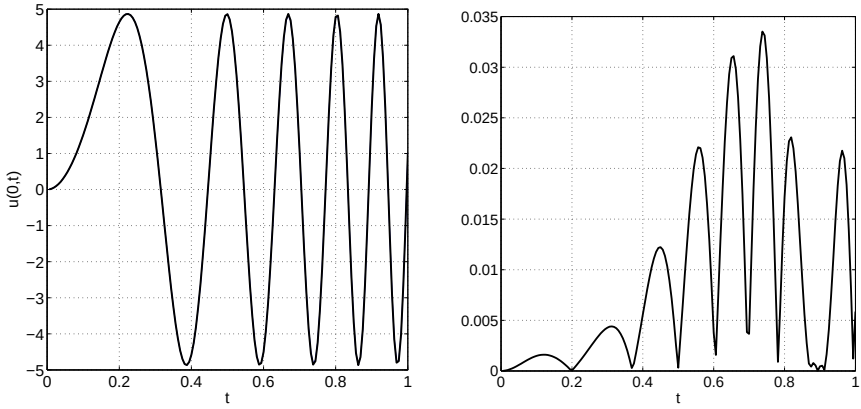

FIGURE 10. Analytical solution and relative error obtained by energetic BEM with $c = 1$, $P = 1000$, $D = 0$ and $\Delta t = 0.00625$.

$u(0,t)$. The relative errors E_s defined in equation (5.2) increase with increasing order of magnitude of P because of the introduction of a region with severe changes in gradient, see Figure 10, but the rate of convergence is substantially equal to 2 independently from the choice of value P. In this case, the computation of integrals involving the fundamental solution becomes more and more challenging because of the alternating signs in the Bessel function addends, see equation (2.6).

If the Péclet number

$$\mathrm{Pe}_P := P\Delta t^2/6 > 1,$$

as in Figure 11, no instabilities appear, but the time step is not suitable for catching all oscillations of the exact solution.

Now considering $\widetilde{u}(0,\cdot)$ obtained by energetic FEM (see Table 9), the accuracy is lower as also expected in this case, and the rate of convergence tends to order 1 as estimated in **[6]**. Analyzing the behavior of the numerical solution over the entire domain $\Omega \times [0,1]$ (Figures 13, 15), we note that the maximum relative error is higher in regions with higher gradient. However, with energetic formulation, FEM keeps its stability as well for large P and without respect to any CFL condition, Figure 16, even if (refer to Table 10) when P is large

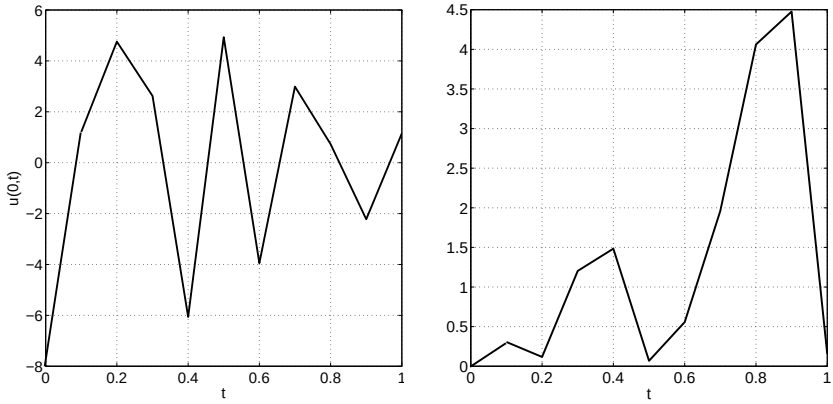

FIGURE 11. Approximate solution and relative error obtained by energetic BEM with $c = 1$, $P = 1000$, $D = 0$ and $\Delta t = 0.1$.

TABLE 8. L_2 relative errors E_s of BEM solution with respect to the analytical solution (5.3) at $x = 0$ and $\mathcal{E}_s := \log_2(E_{s-1}/E_s)$.

BEM

$\Delta t = 0.1 \times 2^{-s}$

	$P = 10^{-1}$		$P = 1$		$P = 10$		$P = 100$	
s	E_s	$\mathcal{E}_s$	E_s	$\mathcal{E}_s$	E_s	$\mathcal{E}_s$	E_s	$\mathcal{E}_s$
0	$4.1{\cdot}10^{-5}$		$4.0{\cdot}10^{-4}$		$3.1{\cdot}10^{-3}$		$7.2{\cdot}10^{-2}$	
1	$1.0{\cdot}10^{-5}$	2.0	$9.9{\cdot}10^{-5}$	2.0	$7.8{\cdot}10^{-4}$	2.0	$2.0{\cdot}10^{-2}$	1.9
2	$2.6{\cdot}10^{-6}$	2.0	$2.5{\cdot}10^{-5}$	2.0	$1.9{\cdot}10^{-4}$	2.0	$5.1{\cdot}10^{-3}$	2.0
3	$6.5{\cdot}10^{-7}$	2.0	$6.2{\cdot}10^{-6}$	2.0	$4.8{\cdot}10^{-5}$	2.0	$1.3{\cdot}10^{-3}$	2.0
4	$1.6{\cdot}10^{-7}$	2.0	$1.6{\cdot}10^{-6}$	2.0	$1.3{\cdot}10^{-5}$	1.9	$3.2{\cdot}10^{-4}$	2.0

we need to refine the time grid more than the space grid in order to improve accuracy and to capture all the oscillations of the exact solution. Considering either CFD or IFD, accuracy of order 2 remains (see Tables 11 and 13, respectively). As expected, the solution obtained with CFD is affected by huge instabilities when the CFL condition is not verified; therefore, the upper triangular portion of Table 12 is empty. On the contrary, these instabilities do not appear with the IFD

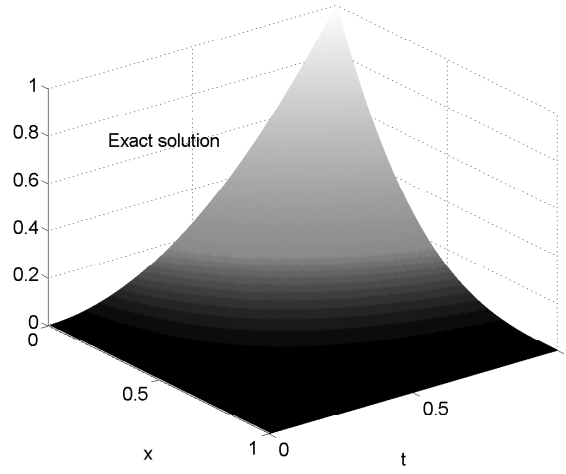

FIGURE 12. Exact solution (5.3) with $c = 1$ and $P = 0.1$.

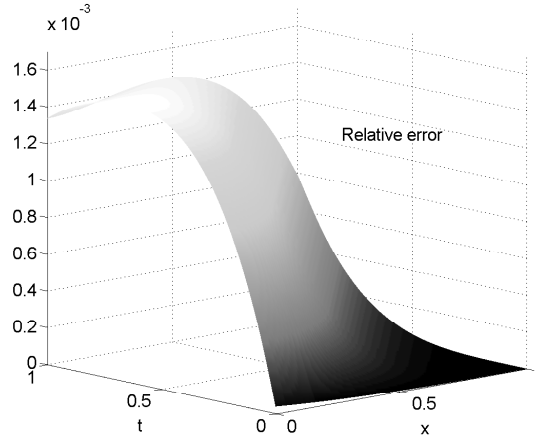

FIGURE 13. Relative error with respect to the solution in Figure 12 obtained by energetic FEM with $\Delta t = \Delta x = 0.00625$.

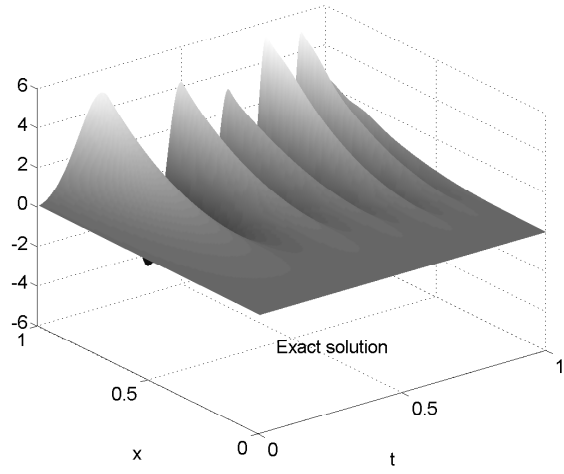

FIGURE 14. Exact solution (5.3) with $c = 1$ and $P = 1000$.

TABLE 9. L_2 relative errors E_s of FEM solution with respect to the analytical solution (5.3) at $x = 0$ and $\mathcal{E}_s := \log_2(E_{s-1}/E_s)$.

FEM

$\Delta t = \Delta x = 0.1 \times 2^{-s}$

	$P = 10^{-1}$		$P = 1$		$P = 10$		$P = 100$	
s	E_s	$\mathcal{E}_s$	E_s	$\mathcal{E}_s$	E_s	$\mathcal{E}_s$	E_s	$\mathcal{E}_s$
0	$3.8{\cdot}10^{-2}$		$3.1{\cdot}10^{-2}$		$1.5{\cdot}10^{-1}$		$6.2{\cdot}10^{-1}$	
1	$2.1{\cdot}10^{-2}$	0.86	$1.7{\cdot}10^{-2}$	0.87	$8.5{\cdot}10^{-2}$	0.84	$4.4{\cdot}10^{-1}$	0.48
2	$1.1{\cdot}10^{-2}$	0.94	$8.9{\cdot}10^{-3}$	0.93	$4.5{\cdot}10^{-2}$	0.93	$2.7{\cdot}10^{-1}$	0.74
3	$5.6{\cdot}10^{-3}$	0.97	$4.5{\cdot}10^{-3}$	0.97	$2.3{\cdot}10^{-2}$	0.96	$1.5{\cdot}10^{-1}$	0.87
4	$2.8{\cdot}10^{-3}$	0.98	$2.3{\cdot}10^{-3}$	0.98	$1.2{\cdot}10^{-2}$	0.98	$7.6{\cdot}10^{-2}$	0.94

method; however, looking at the upper triangular part of Table 7, we observe that no significant improvements are achieved by refining in space.

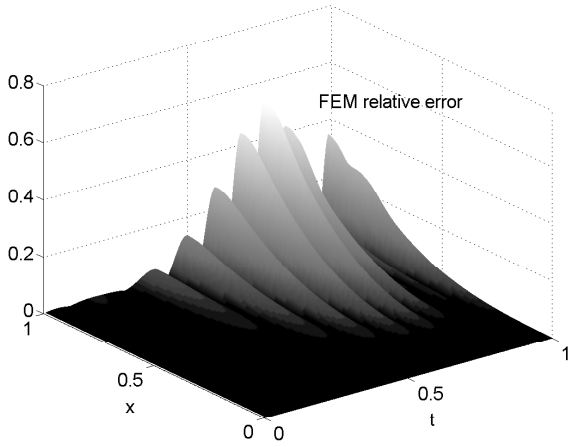

FIGURE 15. Relative error with respect to the solution in Figure 14 obtained by energetic FEM with $\Delta t = \Delta x = 0.00625$.

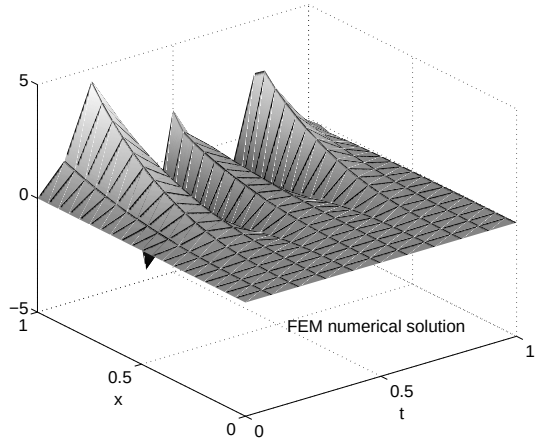

FIGURE 16. Approximate solution in Figure 14 obtained by energetic FEM with $\Delta t = 0.1$, $\Delta x = 0.05$.

TABLE 10. Maximum relative errors of FEM solution with respect to the analytical solution (5.3) over the entire grid, for $P = 100$.

Δt \ Δx	0.1	0.05	0.025	0.0125	0.00625
0.1	1.06	1.04	1.04	1.04	1.04
0.05	$7.71{\cdot}10^{-1}$	$7.67{\cdot}10^{-1}$	$7.67{\cdot}10^{-1}$	$7.68{\cdot}10^{-1}$	$7.68{\cdot}10^{-1}$
0.025	$4.72{\cdot}10^{-1}$	$4.69{\cdot}10^{-1}$	$4.69{\cdot}10^{-1}$	$4.69{\cdot}10^{-1}$	$4.69{\cdot}10^{-1}$
0.0125	$2.60{\cdot}10^{-1}$	$2.59{\cdot}10^{-1}$	$2.58{\cdot}10^{-1}$	$2.58{\cdot}10^{-1}$	$2.58{\cdot}10^{-1}$
0.00625	$1.37{\cdot}10^{-1}$	$1.36{\cdot}10^{-1}$	$1.35{\cdot}10^{-1}$	$1.35{\cdot}10^{-1}$	$1.35{\cdot}10^{-1}$

TABLE 11. L_2 relative errors E_s of CFD solution with respect to the analytical solution (5.3) at $x = 0$ and $\mathcal{E}_s := \log_2(E_{s-1}/E_s)$.

CFD

$\Delta t = \Delta x = 0.1 \times 2^{-s}$

	$P = 10^{-1}$		$P = 1$		$P = 10$		$P = 100$	
s	E_s	$\mathcal{E}_s$	E_s	$\mathcal{E}_s$	E_s	$\mathcal{E}_s$	E_s	$\mathcal{E}_s$
0	$2.6{\cdot}10^{-3}$		$1.1{\cdot}10^{-3}$		$1.1{\cdot}10^{-2}$		$3.8{\cdot}10^{-1}$	
1	$6.6{\cdot}10^{-4}$	2.0	$2.8{\cdot}10^{-4}$	1.9	$2.4{\cdot}10^{-3}$	2.2	$6.7{\cdot}10^{-2}$	2.5
2	$1.6{\cdot}10^{-4}$	2.0	$7.1{\cdot}10^{-5}$	2.0	$5.8{\cdot}10^{-4}$	2.0	$1.6{\cdot}10^{-2}$	2.1
3	$4.1{\cdot}10^{-5}$	2.0	$1.8{\cdot}10^{-5}$	2.0	$1.4{\cdot}10^{-4}$	2.0	$3.8{\cdot}10^{-3}$	2.0
4	$1.0{\cdot}10^{-5}$	2.0	$4.5{\cdot}10^{-6}$	2.0	$3.6{\cdot}10^{-5}$	2.0	$9.5{\cdot}10^{-4}$	2.0

TABLE 12. Maximum relative errors of CFD solution with respect to the analytical solution (5.3) over the whole grid, for $P = 100$.

Δt \ Δx	0.1	0.05	0.025	0.0125	0.00625
0.1	$7.32{\cdot}10^{-1}$				
0.05	$1.31{\cdot}10^{-1}$	$1.24{\cdot}10^{-1}$			
0.025	$3.20{\cdot}10^{-2}$	$2.82{\cdot}10^{-2}$	$2.77{\cdot}10^{-2}$		
0.0125	$9.22{\cdot}10^{-3}$	$7.22{\cdot}10^{-3}$	$6.83{\cdot}10^{-3}$	$6.7{\cdot}10^{-3}$	
0.00625	$3.63{\cdot}10^{-3}$	$2.07{\cdot}10^{-3}$	$1.77{\cdot}10^{-3}$	$1.70{\cdot}10^{-3}$	$1.69{\cdot}10^{-3}$

Analyzing the behavior of the numerical solution over the entire domain $\Omega \times [0, 1]$ (Figures 17–19), one can observe how the magnitude of P significantly influences the choice of discretization parameters.

TABLE 13. L_2 relative errors E_s of IFD solution with respect to the analytical solution (5.3) at $x = 0$ and $\mathcal{E}_s := \log_2(E_{s-1}/E_s)$.

IFD

$\Delta t = \Delta x = 0.1 \times 2^{-s}$

	$P = 10^{-1}$		$P = 1$		$P = 10$		$P = 100$	
s	E_s	$\mathcal{E}_s$	E_s	$\mathcal{E}_s$	E_s	$\mathcal{E}_s$	E_s	$\mathcal{E}_s$
0	$1.6{\cdot}10^{-2}$		$1.5{\cdot}10^{-2}$		$1.0{\cdot}10^{-2}$		$4.4{\cdot}10^{-1}$	
1	$4.4{\cdot}10^{-3}$	1.9	$3.9{\cdot}10^{-3}$	1.9	$2.5{\cdot}10^{-3}$	2.0	$1.3{\cdot}10^{-1}$	1.7
2	$1.1{\cdot}10^{-3}$	2.0	$1.0{\cdot}10^{-3}$	2.0	$6.4{\cdot}10^{-4}$	2.0	$3.6{\cdot}10^{-2}$	1.9
3	$2.9{\cdot}10^{-4}$	2.0	$2.6{\cdot}10^{-4}$	2.0	$1.6{\cdot}10^{-4}$	2.0	$9.1{\cdot}10^{-3}$	2.0
4	$7.3{\cdot}10^{-5}$	2.0	$6.5{\cdot}10^{-5}$	2.0	$4.0{\cdot}10^{-5}$	2.0	$2.3{\cdot}10^{-3}$	2.0

TABLE 14. Maximum relative errors of IFD solution with respect to the analytical solution (5.3) over the whole grid, for $P = 100$.

Δt \ Δx	0.1	0.05	0.025	0.0125	0.00625
0.1	$5.67{\cdot}10^{-1}$	$5.45{\cdot}10^{-1}$	$5.42{\cdot}10^{-1}$	$5.42{\cdot}10^{-1}$	$5.42{\cdot}10^{-1}$
0.05	$2.10{\cdot}10^{-1}$	$2.05{\cdot}10^{-1}$	$2.04{\cdot}10^{-1}$	$2.04{\cdot}10^{-1}$	$2.04{\cdot}10^{-1}$
0.025	$5.62{\cdot}10^{-2}$	$5.56{\cdot}10^{-2}$	$5.56{\cdot}10^{-2}$	$5.56{\cdot}10^{-2}$	$5.56{\cdot}10^{-2}$
0.0125	$1.32{\cdot}10^{-2}$	$1.38{\cdot}10^{-2}$	$1.40{\cdot}10^{-2}$	$1.41{\cdot}10^{-2}$	$1.41{\cdot}10^{-2}$
0.00625	$2.45{\cdot}10^{-3}$	$3.24{\cdot}10^{-3}$	$3.46{\cdot}10^{-3}$	$3.52{\cdot}10^{-3}$	$3.53{\cdot}10^{-3}$

Example 5.3. In the following, we present several simulations related to long-time behavior of the energetic approach. This analysis can be carried out by either increasing the propagation velocity c, keeping $T = 1$, or fixing $c = 1$ and extending the time interval of observation.

• For a problem analogous to that of Example 5.1, where we have set $c = 5$ and $D = 100$ in equation (5.1), the shape of the analytical solution $u(0, t)$ displayed on the left in Figure 1 is expected to be reconstructed in this case within the time interval $[0, 1/c] = [0, 0.2]$ (Figure 20). This solution is recovered by BEM using $\Delta t = 0.00625/c = 0.00125$ with the relative errors displayed in Figure 21 on the left, and it is obtained by FEM using $\Delta t = \Delta x = 0.00125$ with relative error displayed in Figure 21 on the right.

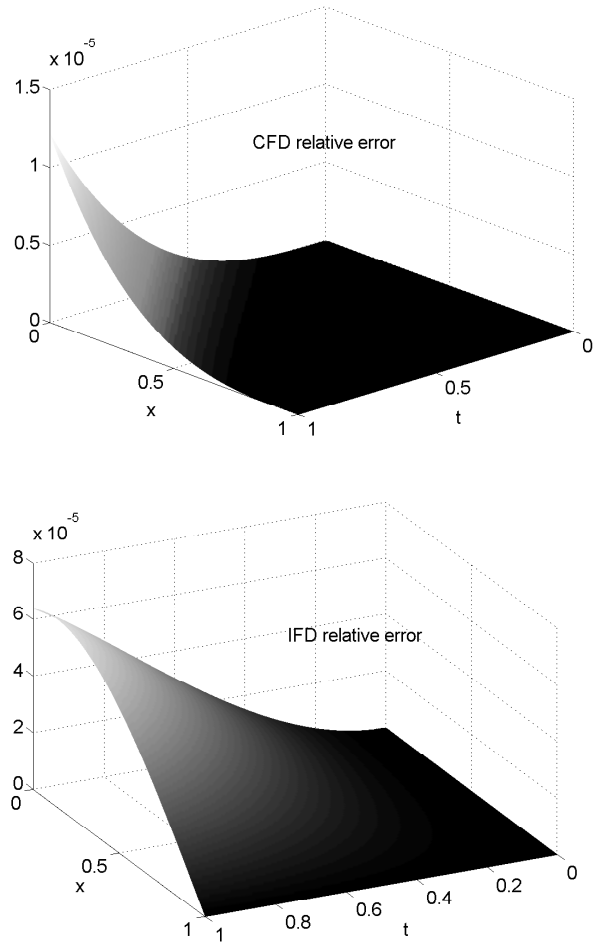

FIGURE 17. Relative error with respect to the exact solution (represented in Figure 12) obtained by CFD (above) and by IFD (below) with $\Delta t = \Delta x = 0.00625$.

• In order to check the long-time behavior of the energetic approach, the problem of Example 5.2 is taken into account here, extending the observation time interval to $[0, 5]$ and fixing $P = 1$.

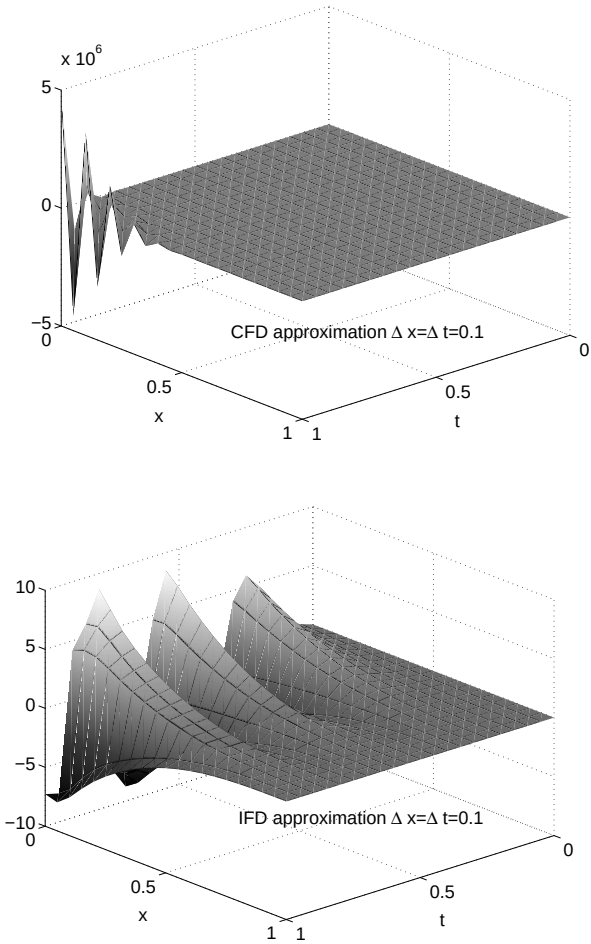

FIGURE 18. Approximate solution when $c = 1$, $P = 1000$, $D = 0$ obtained by CFD (above) and by IFD (below) with $\Delta t = \Delta x = 0.1$.

The BEM approximate solution at $x = 0$ obtained using $\Delta t = 0.00625$ recovers the exact solution (5.3) displayed in Figure 22 with the relative error displayed in Figure 23 on the left. The solution $u(0, t)$ is approximated by FEM using $\Delta t = \Delta x = 0.00625$ with relative

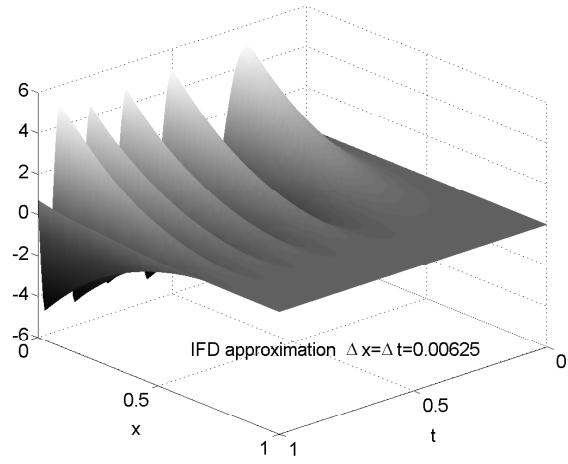

FIGURE 19. Approximate solution when $c = 1$, $P = 1000$, $D = 0$ obtained by IFD with $\Delta t = \Delta x = 0.00625$ (the analogous CFD approximated solution is obtained with $\Delta t = \Delta x = 0.1/2^7$).

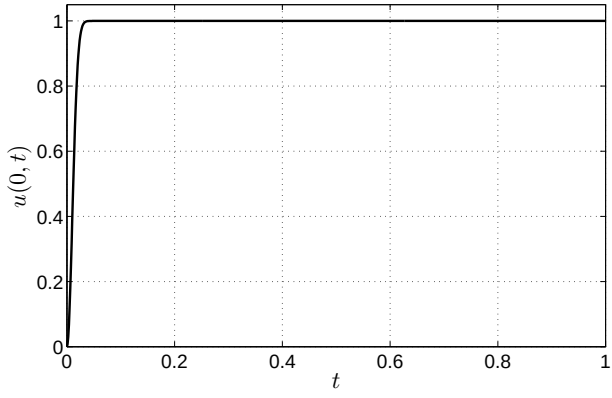

FIGURE 20. Analytical solution (5.1) with $c = 5$ and $D = 100$.

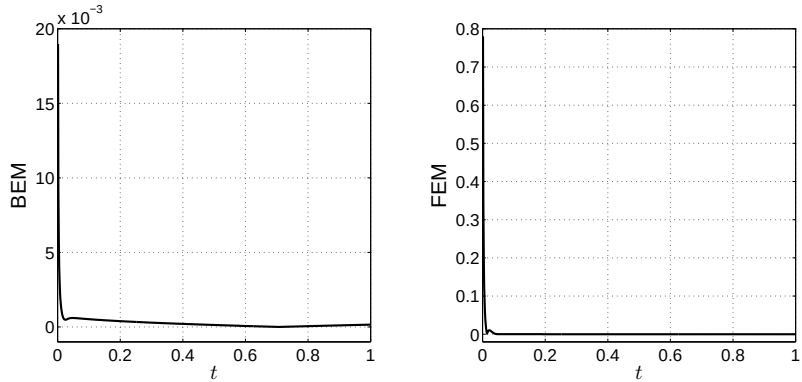

FIGURE 21. Relative errors with respect to the solution represented in Figure 20 obtained by energetic BEM (on the left) and by energetic FEM (on the right).

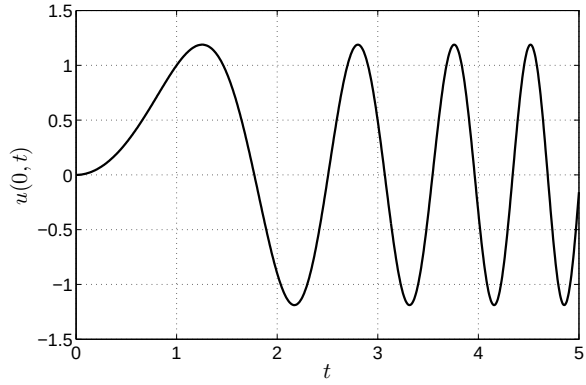

FIGURE 22. Analytical solution (5.3) with $c = 1$ and $P = 1$.

error displayed in Figure 23 on the right. This numerical example is particularly challenging because of the increasing oscillations in time which would require a grid refinement dependent on time marching; however, the energetic BEM and FEM formulations confirm their robustness despite a time growth of the error.

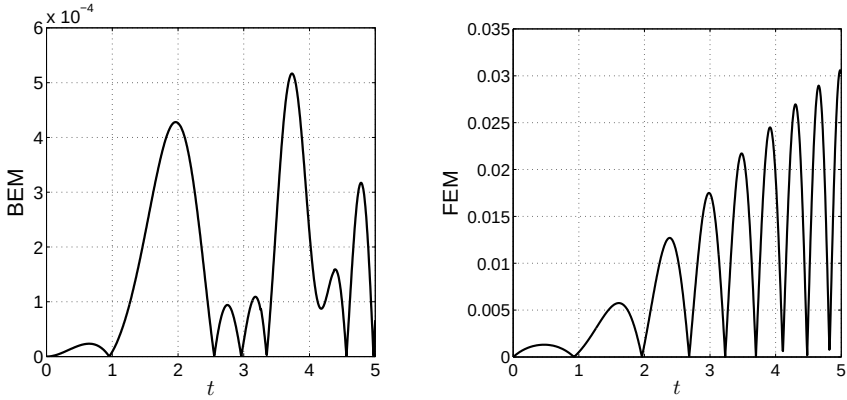

FIGURE 23. Relative errors with respect to solution (5.3) represented in Figure 22 obtained by energetic BEM (on the left) and by energetic FEM (on the right).

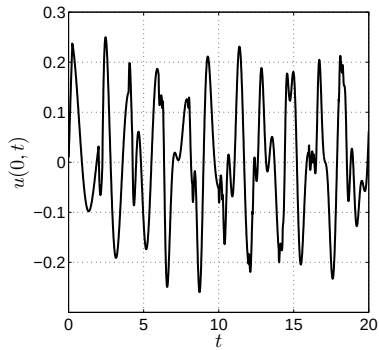

FIGURE 24. Approximate solution, for $c = 1$, $D = 0$, with $P = 10$.

Remark 5.4. In both of the above simulations, energetic BEM maintains its superiority with respect to energetic FEM, concerning accuracy, as already shown in Examples 5.1 and 5.2.

• Here, fixing $L = 1$, $c = 1$ and $T = 20$, we analyze the long-time behavior of the energetic BEM, considering an example found in literature which is equipped by irregular data. In particular, in **[24]**, problem (2.1)–(2.3) is related to a rod fixed at the right end-point $x = L$ (i.e., the Dirichlet condition is $\overline{u}(t) = 0$), subjected to a traction $\overline{p}(t)$

applied at the left end-point $x = 0$, while the right-end side of the PDE is trivial, i.e., $f(x,t) = 0$. For this kind of configuration, the analytical solution, useful for comparison with numerical results, is known for all $x \in \Omega$ and for all $t \in [0,T]$,

$$u(x,t) = \sum_{n=1}^{+\infty} (-1)^{n-1} \times \int_0^{+\infty} 2\big[G\big(x,-2(n-1)L;t-\tau\big) - G\big(x,2nL;t-\tau\big)\big]\overline{p}(\tau)d\tau, \tag{5.4}$$

where $G(x,\xi;t-\tau)$ is defined as in equation (2.5).

In order to investigate the effect of material damping in structures, a single pulse traction

$$\overline{p}(t) = H[t] - H[t-1/4],$$

as in **[24]**, is applied.

TABLE 15. Table of errors in L^2-norm in time, with respect to the analytical solution (5.4) at $x = 0$.

Δt	$P = 10$
0.2	$3.07 \cdot 10^{-1}$
0.1	$1.14 \cdot 10^{-1}$
0.05	$3.11 \cdot 10^{-2}$
0.025	$8.47 \cdot 10^{-3}$

In Figure 24, $u(0,t)$ has been computed by energetic BEM, using $\Delta t = 0.01$, assuming $D = 0$ and $P = 10$: the approximation overlaps the analytical solution. Furthermore, Table 15 shows the convergence towards the analytical solution (5.4), using $L^2([0,1])$-norm in time and refining the discretization parameter Δt. We note that no instabilities appear, and the approximate solution is in agreement with the exact one while considering a much longer (quintuple) time interval than that investigated in **[24]**.

• Finally, we consider, fixing $L = 1$, $c = 1$, $D = 10$, $P = 0$, a set of data for which the analytical solution of problem (2.1)–(2.3) is $u(x,t) = c^2t^2(1-x)^3$, in the time interval $[0,20]$. The approximate

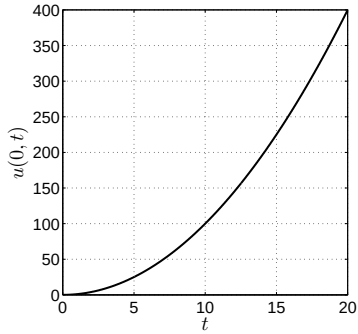

FIGURE 25. Approximate solution, for $c = 1$, $D = 10$, $P = 0$.

TABLE 16. Table of errors in L^2-norm in time, with respect to the analytical solution at $x = 0$.

$\Delta t = \Delta x$	$D = 10$
0.2	$8.47 \cdot 10^{+0}$
0.1	$2.12 \cdot 10^{+0}$
0.05	$5.30 \cdot 10^{-1}$
0.025	$1.30 \cdot 10^{-1}$

solution obtained using $\Delta t = \Delta x = 0.01$ in Figure 25 overlaps the analytical one. In Table 16, we can observe the energetic FEM convergence refining the discretization parameters over a large time interval, even with a higher rate than expected, due to the polynomial nature of the data and the solution.

6. Conclusions. In this paper, we have analyzed, from a numerical point of view, the energetic BEM and FEM separately, applied to the solution of 1D damped wave propagation problems in bounded domains, and we have compared these methods with classical finite differences schemes, both implicit and explicit.

Summarizing the results obtained, we can state the superiority of the energetic approaches concerning stability even under large values of damping parameters and without respect to any CFL condition, which

instead affects explicit domain methods. Furthermore, the simulations related to the long-time behavior of energetic BEM and FEMs have revealed that they are stable and convergent even on large time intervals of analysis.

Due to their optimal performances, we are currently studying an extension for the numerical solution of damped wave propagation problems in 2D space dimension.

REFERENCES

1. A. Aimi, L. Desiderio, M. Diligenti and C. Guardasoni, *A numerical study of energetic* BEM-FEM *applied to wave propagation in* 2D *multidomains*, Publ. Inst. Math. **96** (2014), 5–22.

2. A. Aimi and M. Diligenti, *A new space-time energetic formulation for wave propagation analysis in layered media by* BEMs, Int. J. Numer. Meth. Eng. **75** (2008), 1102–1132.

3. A. Aimi, M. Diligenti, A. Frangi and C. Guardasoni, *Energetic* BEM-FEM *coupling for wave propagation in* 3D *multidomains*, Int. J. Numer. Meth. Eng. **97** (2014), 377–394.

4. A. Aimi, M. Diligenti and C. Guardasoni, *Energetic* BEM-FEM *coupling for the numerical solution of the damped wave equation*, Adv. Comp. Math. (2016), doi:10.1007/s10444-016-9500-1.

5. A. Aimi, M. Diligenti, C. Guardasoni and S. Panizzi, *Energetic* BEM-FEM *coupling for wave propagation in layered media*, Comm. Appl. Indust. Math., DOI:10.1685/journal.caim.438, 2013.

6. A. Aimi and S. Panizzi, BEM-FEM *coupling for the* 1D *Klein-Gordon equation*, Numer. Meth. Part. Diff. Equat. **30** (2014), 2042–2082.

7. H. Antes, G. Beer and W. Moser, *Soil-structure interaction and wave propagation problems in* 2D *by a Duhamel integral based approach and the convolution quadrature method*, Comp. Mech. **36** (2005), 431–443.

8. A. Bachelot, L. Bounhoure and A. Pijols, *Couplage éléments finis–potentiels retardés pour la diffraction électromagnétique par un obstacle hétérogène*, Numer. Math. **89** (2001), 257–306.

9. A. Bamberger and T. Ha Duong, *Formulation variationelle espace-temps pour le calcul par potential retardé de la diffraction d'une onde acoustique* (I), Math. Meth. Appl. Sci. **8** (1986), 405–435.

10. ———, *Formulation variationelle pour le calcul de la diffraction d'une onde acoustique par une surface rigide*, Math. Meth. Appl. Sci. **8** (1986), 598–608.

11. M. Costabel, *Time-dependent problems with the boundary integral equation method*, in *Encyclopedia of computational mechanics*, E. Stein, et al., eds., John Wiley and Sons, New York, 2004.

12. T.A. Cruse and F.J. Rizzo, *A direct formulation and numerical solution of the general transient elastodynamic problem*-I, J. Math. Anal. Appl. **22** (1968), 244–259.

13. A. Frangi, *Elastodynamics by* BEM: *A new direct formulation*, Inter. J. Numer. Meth. Eng. **45** (1999), 721–740.

14. A. Frangi and G. Novati, *On the numerical stability of time-domain elastodynamic analyses by* BEM, Comp. Meth. Appl. Mech. Eng. **173** (1999), 403–417.

15. T. Ha Duong, *On retarded potential boundary integral equations and their discretization*, *Topics in computational wave propagation*, *Direct and inverse problems*, P. Davies, et al., eds., Springer-Verlag, New York, 2003.

16. G.M. Hulbert and T.J.R. Hughes, *Space-time finite element methods for second-order hyperbolic equations*, Comp. Meth. Appl. Mech. Eng. **84** (1990), 327–348.

17. C. Lubich, *Convolution quadrature and discretized operational calculus*, I, Numer. Math. **52** (1988), 129–145.

18. ———, *Convolution quadrature and discretized operational calculus*, II, Numer. Math. **52** (1988), 413–425.

19. G. Maier, M. Diligenti and A. Carini, *A variational approach to boundary element elasto-dynamic analysis and extension to multidomain problems*, Comp. Meth. Appl. Mech. Eng. **92** (1991), 193–213.

20. A. Quarteroni and A. Valli, *Numerical approximation of partial differential equations*, Springer-Verlag, New York, 1994.

21. G.R. Richter, *An explicit finite element method for the wave equation*, Appl. Numer. Math. **16** (1994), 65–80.

22. F.J. Sayas, *Energy estimates for Galerkin semidiscretizations of time domain boundary integral equations*, Numer. Math. **124** (2013), 121–149.

23. M. Schanz, *Application of* 3D *boundary element formulation to wave propagation in poroelastic solids*, Eng. Anal. Bound. Elem. **25** (2001), 363–376.

24. A. Vick and R.L. West, *Analysis of damped wave using the boundary element method*, Trans. Model. Simul. **15** (1997), 265–278.

University of Parma, Department of Mathematical, Physical and Computer Sciences, Parma 43124, Italy
Email address: **alessandra.aimi@unipr.it**

University of Parma, Department of Mathematical, Physical and Computer Sciences, Parma 43124, Italy
Email address: **mauro.diligenti@unipr.it**

University of Parma, Department of Mathematical, Physical and Computer Sciences, Parma 43124, Italy
Email address: **chiara.guardasoni@unipr.it**